OPTIMIZATION AND CHARACTERIZATION OF ADDITIVELY MANUFACTURED INJECTORS FOR A SMALL-SCALE GAS/GAS THRUSTER

J. Caspar*, T. Fiedler[†], C. Bauer [‡], T. Stelzer*, S. Silvestri*

* TU Braunschweig, Institute of Space Systems, Hermann-Blenk-Str. 23, 38108 Braunschweig, Germany
 † TU Braunschweig, Institute for Materials Science, Langer Kamp 8, 38106 Braunschweig, Germany
 ‡ DeltaOrbit GmbH, Lichtenbergstr. 6, 85748 Garching, Germany

Abstract

The growing demand for mega-constellations, in-orbit servicing, and lunar missions necessitates advancements in space-craft propulsion. Cryogenic propellants, such as methane and oxygen, offer an alternative that is more efficient and environmentally friendly than conventional storable propellants. Injectors have a significant impact on the performance, combustion stability, and reliability of rocket engines. To design injectors that meet these demanding requirements, additive manufacturing can be used to enable innovative designs. While Inconel has often been used due to its high tensile strength and temperature resistance, copper-based alloys, which have only recently become available for additive manufacturing, may offer advantages due to their high thermal conductivity. In this paper, the design process of injectors for a small-scale gas/gas thruster is presented, focusing on manufacturability as well as injector performance. Additive manufacturing, namely laser power-bed fusion, yields the possibility to design components with complex internal geometries in an integral design, potentially reducing the number and mass of required components. However, the resulting parts exhibit anisotropic material properties, as well as surface properties depending on surface orientation. As the surface roughness directly impacts the flow characteristics in an injector, these special aspects of additive manufacturing are given particular consideration in the design. Four different injector types are manufactured and subjected to cold-flow testing.

KeywordsInjector; In-space propulsion; Additive manufacturing; Copper alloys

NOMENCLATURE		φ	Angle coordinate	rad	
Symbols			ho	Density	kg/m^3
A	Area	m^2	θ	Swirl half-cone angle	deg
C_d	Discharge coefficient				
D	Diameter	m	Indices		
F	Thrust	N	СВ	Central body	
J	Momentum flux ratio		С	Chamber / constriction	
L	Length coordinate	m	dyn	Dynamic	
\dot{m}	Mass flow rate	kg/s	eq	Equivalent	
MW	Molecular weight	kg/mol	eql	Equilibrium	
n,N	Number		f	Fuel	
r, R	Radius	m	init	Initial	
Re	Reynolds number		inj	Injector exit	
T	Temperature	K	0	Oxidizer	
t	Wall thickness	m	tot	Total	
V	Velocity	m/s	Abbrevi	ations	
X	Mole fraction		AM	Additive manufacturing	
α	Golden angle	rad	CEA	Chemical equilibrium with app	dications
δ	Boundary layer thickness	m			
ϕ	Golden ratio		CFD	Computational fluid dynamics	

ESA European Space Agency

FFSC Full-flow staged combustion

GCH4 Gaseous methane GH2

GN₂ Gaseous nitrogen

GO2 Gaseous oxygen

ISTV In-Space Transportation Vehicle

Gaseous hydrogen

NASA National Aeronautics and Space Administra-

PBF-LB/M Laser powder-bed fusion / laser beam melting

1. INTRODUCTION

The current trend in spaceflight development places new demands on spacecraft propulsion systems. For the near 2025 - 2050 horizon, ESA envisions a space transportation ecosystem. In contrast to the traditional approach of utilizing tailored solutions for each mission, this ecosystem would constitute a "hub and spoke" architecture [1]. Reusable, heavy launchers would inject different payloads into high parking orbits from which the "last mile delivery" to the final orbit is realized by In-Space Transportation Vehicles (ISTVs). These spacecraft require efficient, high-performing and reliable propulsion systems that can be reignited.

Another trend is the increased interest in lunar exploration missions. Accelerated by the commitment of several countries to carry out crewed landings on the Moon and NASA's commercialization approach, there have been a large number of developments for lunar landers in recent years. In addition to the common propulsion system requirements, landers usually require extended throttling capabilities to ensure a soft landing.

In-space propulsion systems conventionally utilize storable, hydrazine-based propellant combinations. They have the advantage that they can be easily stored in liquid state at ambient temperature and low pressure. Moreover, hypergolic propellant combinations facilitate the ignition process, reducing engine complexity and mass. However, hydrazine-based propellants achieve a comparably low specific impulse and they are highly toxic, posing environmental risk and increasing the cost of ground procedures. Cryogenic fuels, namely liquid methane, hydrogen, and oxygen, provide a promising alternative. While they have been used for launch vehicles for a long time due to their high specific impulse, recent research focuses on their application for in-space propulsion. Challenges such as the more complex ignition, storage and propellant management are the subject of current research.

The injector of a rocket engine is responsible for the efficient atomization and precise mixing of propellants, and has thus a great influence on the overall efficiency, performance, and reliability of an engine. While much research on injector characterization and optimization addressed conditions akin to launcher applications, different approaches might be promising for in-space engines, and various injector types have the potential to combine high efficiency and reliability. While this is not typical for launcher engines, the injection of both fuel and oxidizer in their gaseous state might allow

for efficient designs, when combined with innovative cycles for in-space propulsion.

Additive manufacturing (AM) of rocket engines yields advantages, compared to conventional manufacturing techniques. It allows for the reduction in part count and mass through increased design freedom, as fewer manufacturing constraints are imposed, enabling complex internal flow geometries. The overall processing time and cost can be reduced, which facilitates rapid prototyping for design iterations. A broad range of metal alloys can be used for AM. For space propulsion, mostly nickel-chromium based alloys, such as Inconel, have been utilized due to their high temperature strength, oxidation resistance, and good processability using AM [2-4]. Copper-based alloys are an interesting alternative. Due to their high thermal conductivity, copper alloys are used in rocket engine combustion chambers, where high thermal gradients and heat fluxes are present. Although the AM of copper alloys proves to be challenging, recent advancements facilitate the manufacturing of copper structures [5]. More specifically, this study focuses on the alloy CuCr1Zr (material number CW106C), which yields both high thermal conductivity and good hardenability. The components are manufactured using laser powder-bed fusion (PBF-LB/M).

This work covers the dimensioning, design and manufacturing of four different injector types for a small, 500N-class thruster, utilizing gaseous oxygen (GO2) and methane (GCH4). All injectors are integral designs with an identical external envelope. Different injector types are implemented, resulting in varying internal propellant flow and faceplate geometries. This approach facilitates the rapid swapping of injectors in the test setup, enabling targeted parameter studies and rapid prototyping.

The design for AM of the injectors is aimed at an assembly in a research thruster. However, the findings of the design process are just as applicable to flight hardware. By designing and manufacturing four different injector types with varying complexity, the possibilities and limitations of the PBF-LB/M process utilizing copper alloys for rocket engine injectors can be assessed.

2. PERFORMANCE PREDICTION MODEL

Most of the research carried out to date in the field of gaseous injectors has involved characterization either by means of computational fluid dynamics (CFD) or by means of experiments, which in turn can be divided into hot-fire and cold-flow tests. However, the applicability of the models developed here is often limited to a narrow range. This applies, for example, to the element type, the propellant combination, or a specific range of injection velocities and velocity ratios. One exception is a comprehensive study by Calhoon et al. [6], who have developed a general model for performance prediction for gaseous injectors, which is applied in this work.

The background to the 1973 study is the development of the Space Shuttle Auxiliary Propulsion System, for which the utilization of GO2/GH2 was envisaged. The aim was to develop a generally valid model for estimating the mixing efficiency and the combustion efficiency η_{c^*} , which should be generally applicable for different injector element types,

2 @2024

propellant combinations and operating points. For this purpose, a large number of experimental cold-flow tests were carried out with differently dimensioned shear coaxial, swirl, premix, showerhead and impinging injectors with nitrogen and helium. In addition, hot-fire tests of shear coaxial, swirl, premix and impinging injectors with GO2/GH2 were carried out.

Two models with different approaches were formulated on the basis of the rich experimental data. The first model is empirical and directly correlates injector parameters with the test data obtained. The applicability of this model is therefore limited to the fuel combination GO2/GH2, the tested element types and the range of tested operating points. The second model, on the other hand, uses the approach of postulating physical behavior of the system that can explain the observed test data. In addition to its general applicability, this model has the advantage that the design and operating parameter interactions can be identified and that a physical insight into the mixing and combustion process is made possible. Although the model employs simplifications, Calhoon et al. achieved a high level of agreement with the test data.

2.1. Mixing model

The central observation underlying the analytical model of Calhoon et al. is a direct correlation of the dynamic pressure dissipation of the injected gas stream with increased mixing efficiency. The explanation derived from this is that the dynamic pressure dissipated in the axial direction is converted into a radial pressure gradient, which is associated with the distribution and mixing of oxidizer and fuel.

In order to model the dissipation of the dynamic pressure in the axial direction, a stationary potential flow field is assumed, whereby oxidizer and fuel are considered independently. The highly simplified assumption is that the gas initially exits at the injector outlet with a homogeneous velocity profile over the effective cross-section $C_{d,o}A_o$, or $C_{d,f}A_f$. It is assumed that the initial velocity is built up by the static pressure drop during the outlet being completely converted into dynamic pressure in the orifice:

$$V = \frac{\dot{m}}{\rho A C_d}$$

A boundary layer now develops at the periphery of the flow cross-section, which increases with axial length. This is simplified as a fully turbulent flat plate boundary layer:

(2)
$$\delta = \frac{0.375L}{Re_L^{0.2}}$$

For the sake of simplification, the velocity profile is assumed to be a linear function that assumes the value of the original injection velocity at the inner edge of the boundary layer $r=R_0-\delta$ and the value 0 at the outer edge of the boundary layer $r=R_0+\delta$. From the point at which the boundary layer thickness exceeds the radius R_0 , the velocity profile represents a single linear function. Its maximum value is chosen so that the integral of the velocity profile remains constant over the radius. The progression is shown in figure 1 for a circular orifice. Similarly, an annular orifice was modeled in this work. The flow field of the swirl injector is more complex and is described in detail in reference [6].

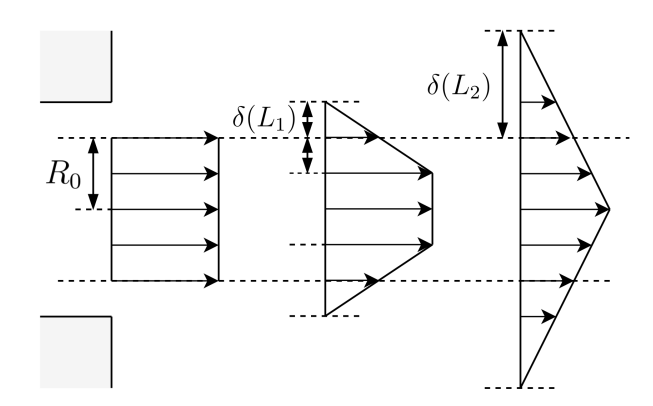


FIG 1. Flow assumptions for a circular cross section, according to Calhoon et al. model [6].

The dynamic pressure in the axial direction corresponds to the integral of the dynamic pressure over the cross-sectional area of the flow, divided by the cross-sectional area. The ratio of the local dynamic pressure to its initial value is therefore

(3)
$$\frac{\Delta P_{dyn}(L)}{\Delta P_{inj}} = \frac{1}{A_c \cdot \Delta P_{inj}} \int_{R_0 - \delta}^{R_0 + \delta} \frac{1}{2} \rho V(r)^2 2\pi r dr$$

This dynamic pressure dissipation is directly correlated with the mole fraction decline:

(4)
$$X(L) = X_{eql} + \frac{\Delta P(L)}{\Delta P_{inj}} \left(\frac{\Delta P_{inj}}{\Delta P_{eq}}\right)^F (X_{init} - X_{eql})$$

The initial mole fraction X_{init} is equal to 1 for non-premix elements and approaches the equilibrium value X_{eql} with the complete degradation of the dynamic pressure.

(5)
$$X_{o,eql} = \frac{\dot{m}_o/MW_o}{\dot{m}_o/MW_o + \dot{m}_f/MW_f}$$

(6)
$$X_{f,eql} = \frac{\dot{m}_f/MW_f}{\dot{m}_o/MW_o + \dot{m}_f/MW_f}$$

As the dynamic pressure is identified to provide the mixing potential, an equivalent dynamic pressure is defined to normalize the respective oxygen/fuel dynamic pressures $\Delta P_{inj,o}, \Delta P_{inj,f}$ at the injector exit:

(7)
$$\Delta P_{eq} = \frac{(\dot{m}_o/MW_o) \cdot \Delta P_{inj,o} + (\dot{m}_f/MW_f) \cdot \Delta P_{inj,f}}{\dot{m}_o/MW_o + \dot{m}_f/MW_f}$$

The element coefficient F is used in the exponent of the ratio $\Delta P/P_eq$. It depends on the element type and describes the ratio of the surface area of the flow field which is available for mixing with the other propellant component to the total surface area. For a shear coaxial element with oxidizer as primary component, $F_o=1$ and $F_f\approx 0.5$, since the outside of the fuel stream is not adjacent to the oxidator stream.

3. INJECTOR DESIGN

3.1. Dimensioning

The injector design encompasses a standardized geometric envelope for all injectors, allowing for the rapid swapping of different element types within the same propellant manifold. While the outer envelope remains constant, the possibilities of AM yield design freedom regarding the internal fuel lines and the injector faceplate geometry.

Four injector designs were chosen for manufacturing: Shear coaxial, central body shear coaxial, showerhead, and swirl. For the dimensioning of the injector faceplate geometry, the respective design features were chosen based on the mixing model described in section 2.1. A detailed description of the dimensioning of each component is given in the following sections.

A standard design point was chosen for all injectors. Based on a nominal thrust of $500\,\mathrm{N}$ at ambient conditions, a CEA calculation was performed [7]. The ensuing parameters for the baseline design point are summarized in table 1. The Rupe mixing efficiency according to reference [8], which is 0 when fuel and oxidizer streams have not mixed and 100 when the local mixture ratios in the fuel and oxidizer streams corresponds to the overall mixture ratio, was evaluated at a chamber length of $0.1\,\mathrm{m}$.

TAB 1. Baseline operation point parameters used for injector dimensioning

500 N
$20\mathrm{bar}$
GO2 / GCH4
$275\mathrm{K}$
$1.786\times10^{-1}\mathrm{kg/s}$
$4.464 \times 10^{-2} \mathrm{kg/s}$
$1.339\times10^{-1}\mathrm{kg/s}$

All shear type injectors were designed for the identical momentum flux ratio as well as identical injection velocities for all injectors, ensuring comparability of all components. The momentum flux ratio is defined as

$$J = \frac{\rho_f V_f^2}{\rho_o V_o^2}.$$

For the selection of an adequate momentum flux ratio and injection speeds that may allow for stable combustion, several studies investigating GO2/GCH4 thrusters were considered [4,9,10]. Based on this data, a momentum flux ratio of J=0.5, a fuel injection velocity of $V_f=150\,\mathrm{m/s}$, and an oxidizer injection velocity of $V_o=152.4\,\mathrm{m/s}$ were chosen for the standard design point. This results in an oxidizer cross-sectional injection area of $A_o=3.057\times10^{-5}\,\mathrm{m^2}$ and a fuel cross-sectional injection area of $A_f=2.006\times10^{-5}\,\mathrm{m^2}$.

3.1.1. Shear coaxial injector

The cold-flow mixing model described in section 2.1 was applied in order to relate the chosen cross-sectional areas in the space of possible solutions for the baseline operation point mentioned above. The integral in equation 3 was solved numerically, instead of using a simplified analytical

solution proposed by Calhoon et al. [6], as a comparison has shown significant deviations for the case considered here. The oxidizer post wall thickness was defined to be $1\ \mathrm{mm}$. This comparably conservative value was chosen with regards to the manufacturability using CuCr1Zr. The discharge coefficients of the oxidizer orifice was approximated with 0.85, the fuel annular orifice with 0.75.

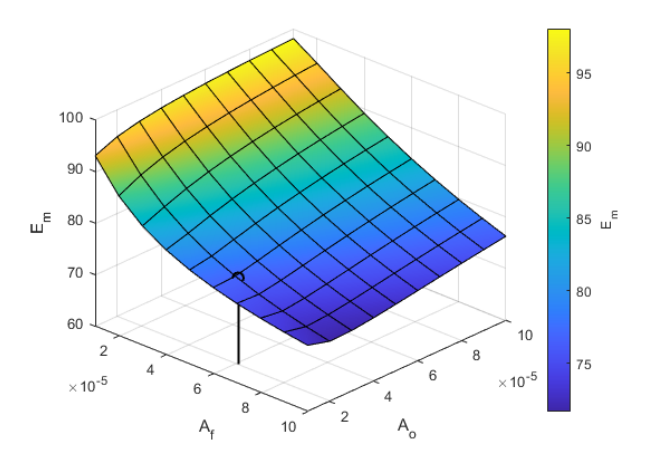


FIG 2. Shear coaxial injector mixing efficiency over oxidizer and fuel injection area. Design point marked as singular value

The goal of applying the mixing model was a comparison of different faceplate geometries from a design standpoint. The parameter used for comparison is the Rupe mixing efficiency. For a shear coaxial design, the oxidizer and fuel injection cross-sectional areas can be varied, resulting in different mixing efficiencies. The results are plotted in figure 2. High mixing performance can be achieved for smaller cross sectional areas. This is due to the higher ratio of the boundary layer to the hydraulic diameter, leading to a more rapid dissipation of the dynamic pressure. In this case, the variation of the oxidizer cross sectional area has the most significant impact on overall mixing performance, as the velocity dissipation in its circular cross section is slower than for an annular geometry with the same area. For the selected cross-sectional areas in this work, a mixing efficiency of $77\,\%$ results. The design point is added in figure 2.

The predicted increase in mixing performance can not be expected to correspond with ever higher combustion performance for very low cross sectional areas. As the mass flow is assumed to be constant, a decreasing cross section leads to an increase of the injection velocity, which can promote unstable combustion behavior at high values. Additionally, the manufacturing process limits the achievable orifice diameter and annulus thickness that can be reliably achieved.

TAB 2. Shear coaxial injector design parameters.

D_o in m	6.240×10^{-3}
t in ${ m m}$	1×10^{-3}
$D_{f,1}$ in m	8.240×10^{-3}
$D_{f,2}$ in ${ m m}$	9.666×10^{-3}

3.1.2. Central body shear coaxial injector

Analogously to the conventional shear coaxial injector, the cold-flow mixing model was applied in order to compare the mixing efficiency E_m for varying oxidizer and fuel injection cross sectional surface areas. Due to the central body restriction, the oxidizer faceplate geometry resembles an annulus, rather than a circle for the conventional shear coaxial injector. This specific element type has not been investigated by Calhoon et al. However, their model remains applicable by modeling the flow of two annular jets.

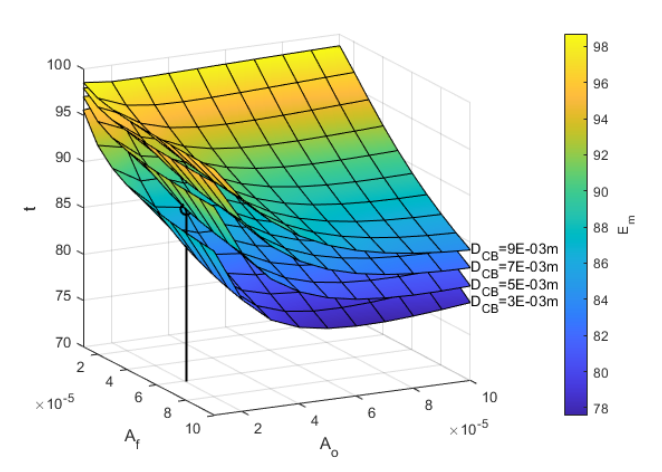


FIG 3. Central body shear coaxial injector mixing efficiency over oxidizer and fuel injection area, plotted for several central body diameters. Design point marked as singular value.

The ensuing mixing efficiency E_m is plotted in figure 3 over varying injection surface areas. Several surfaces are plotted, ensuing the results for varying central body diameters $3\,\mathrm{mm}$, $5\,\mathrm{mm}$, $7\,\mathrm{mm}$ and $9\,\mathrm{mm}$. All surfaces show the same qualitative shape, with higher mixing efficiencies for lower surface areas, corresponding to higher injection velocities and more rapid dissipation of the dynamic pressure. Higher mixing efficiencies can also be achieved with larger central body diameters. According to the model, the injection velocity is not altered by a differing central body diameter for the same surface areas. However, higher restriction diameters correspond to thinner stream annuli, which dissipate more rapidly, thus increasing the mixing efficiency.

For ever decreasing surface areas, the same restrictions already discussed in the previous section apply. In the case, the thickness of oxidizer and fuel annuli is further decreased by the central body. A central body diameter of $5\,\mathrm{mm}$ was chosen due to manufacturing limitations regarding the annulus thickness. For this value, a mixing efficiency of $89\,\%$ is reached.

TAB 3. Central body shear coaxial injector design parameters.

$D_{CB} = D_{o,1}$ in m	5×10^{-3}
$D_{o,2}$ in m	7.996×10^{-3}
t in ${ m m}$	1×10^{-3}
$D_{f,1}$ in ${ m m}$	9.996×10^{-3}
$D_{f,2}$ in ${ m m}$	1.120×10^{-2}

3.1.3. Showerhead injector

The showerhead injector features circular orifices for both oxidizer and fuel injection. Thus, the circular stream can be applied for the cold-flow mixing model. Akin to the previously discussed coaxial injectors, the mixing efficiency increases with decreasing surface areas. As the same surface areas were chosen as for the coaxial type injectors, a remaining design parameter is the number of both fuel and oxidizer orifices, or equivalently, the orifice diameters. Thus, in figure 4, the mixing efficiency is plotted over the varying number of oxidizer and fuel orifices.

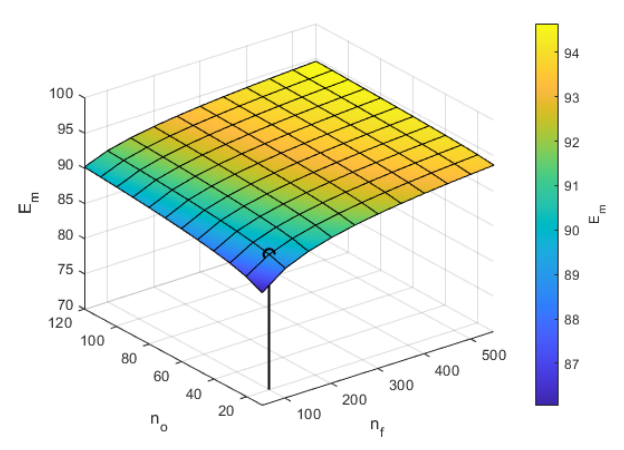


FIG 4. Showerhead injector mixing efficiency over number of oxidizer and fuel orifices. Design point marked as singular value.

A higher mixing efficiency for a larger number of both oxidizer and fuel orifices can be observed, due to the faster dynamic pressure dissipation of smaller jets. For the manufactured showerhead injector, a number of 20 oxidizer orifices and 100 fuel orifices was defined. While the fuel orifice number was limited due to manufacturing considerations, a lower amount of oxidizer orifices had to be chosen, as their fuel lines have to be routed through the fuel dome. A mixing efficiency of $89\,\%$ is predicted.

It must be noted at this point that the Calhoon et al. mixing model is solely based on the dissipation of the dynamic pressure inside the gas jets, which are modeled individually. While good agreement with experimental data was achieved, the model neglects the influence of the positioning of the individual orifices. However, in the case of the showerhead injector, this factor has a significant influence in reality.

For this work, an orifice arrangement was chosen which mimics the positioning of leaves around a stem, or the arrangement of seeds in flowers, found in nature. The same approach was used by Reuter et al. [4] for a gaseous injector utilizing GO2/GCH4. The pattern is constructed using the golden angle $\alpha=\phi/\left(2\pi\right)$ with the golden ratio $\phi=\left(\sqrt{5}+1\right)/2.$ For the positioning of the orifices, a number of points $n=\{1,...,N\},$ with $N=N_o+N_f,$ is placed around a center point at angles $\varphi(n)=n\cdot\alpha.$ The points are placed at radii

(9)
$$r(n) = \sqrt{\varphi(n)} \cdot \frac{r(N)}{\varphi(N)}.$$

This results in a spiral of evenly distributed points $S(\varphi,r)$. In nature, this pattern maximizes the area for an individual seed, or the amount of light for leafs around a stem.

The maximum radius r(N) was defined $0.5\,\mathrm{mm}$ smaller than the chamber radius, which is $34\,\mathrm{mm}$. The resulting pattern still needs to be divided into points for oxidizer and for fuel orifices. To achieve this, a second spiral $S'(\varphi',r')$ with $n'=\{1,...,n_o\}$ was constructed. The outer radius was defined as $r'(n_o)=0.86\cdot r(N)$. Thus, the outer border of the faceplate is not occupied by oxidizer orifices, which leads to a fuel-rich boundary layer. As the positions of the points of both spirals do not coincide, the geometrically closest points to S' in S are chosen for the oxidizer orifices.

TAB 4. Showerhead injector design parameters.

D_o in m	1.4×10^{-3}
D_f in ${ m m}$	5×10^{-4}
n_o	20
n_f	20

3.1.4. Swirl injector

The swirl injector mixing model is more complex, as the impingement of the fuel and oxidizer flows significantly contributes to the mixing. The Calhoon et al. mixing model [6] utilizes a performance parameter, which is used to correlate the injector geometries and operation parameters to the predicted mixing efficiency. Adapting this approach, the mixing efficiency is plotted over the oxidizer and fuel cross-sectional injection area for various swirl angles in figure 5.

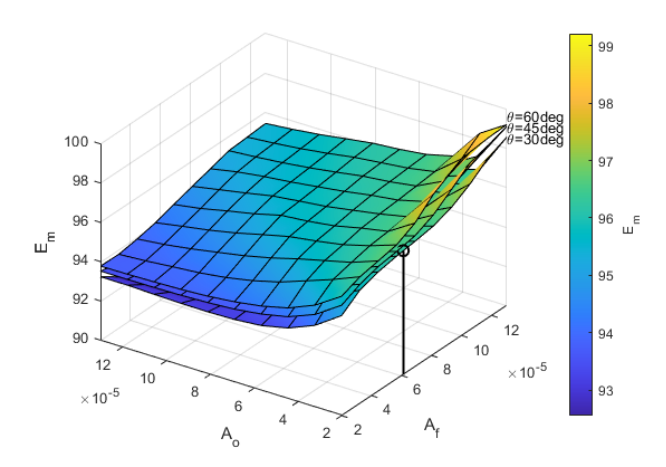


FIG 5. Swirl injector mixing efficiency over oxidizer and fuel injection area, plotted for several swirl angles. Design point marked as singular value.

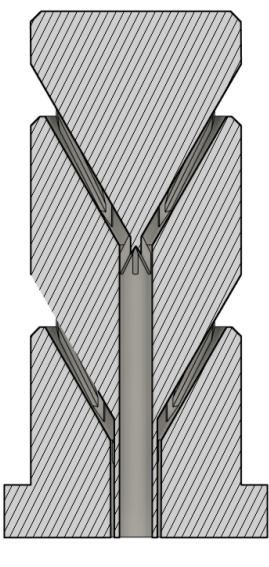
A higher swirl angle intuitively corresponds to a faster mixing and thus a higher mixing efficiency, which is represented by the model. Also, a low oxidizer cross-sectional area in combination with a larger fuel area lead to a high mixing efficiency.

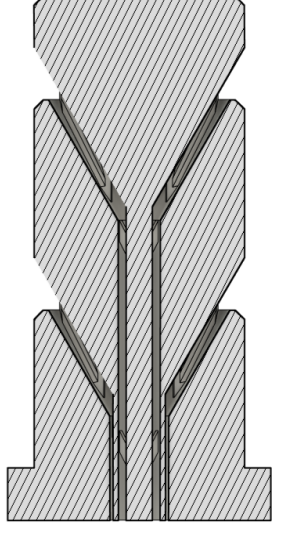
While high swirl angles increase the mixing in rocket engines, they can cause excessive heating of the combustion chamber wall near the injector. For reasons related to the manufacturing of the injectors, which are discussed in detail in the following section, a swirl half-cone angle of 30° was chosen. For this design point, a mixing efficiency of $96\,\%$ is predicted.

TAB 5. Swirl injector design parameters

D_o in ${ m m}$	1.165×10^{-2}
t in ${ m m}$	1×10^{-3}
$D_{f,1}$ in ${ m m}$	1.365×10^{-2}
$D_{f,2}$ in ${ m m}$	1.661×10^{-2}
$ heta$ in $^\circ$	30

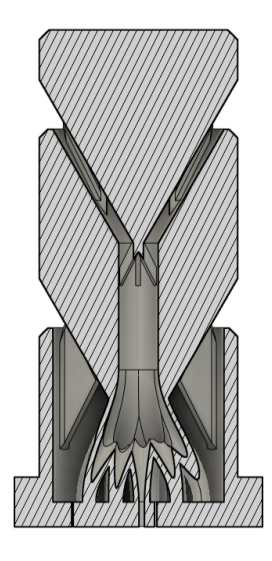
3.2. Mechanical design

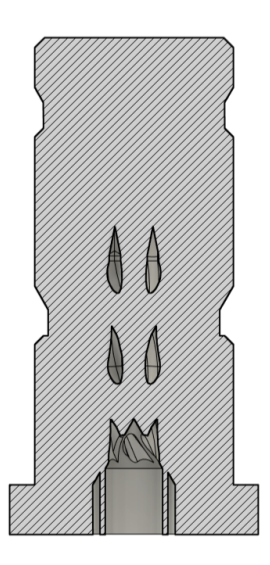




(a) Shear coaxial injector.

(b) Central body shear coaxial iniector.





(c) Showerhead injector.

(d) Swirl injector.

FIG 6. Injector cutaway views.

All injector designs components are made of CuCr1Zr utilizing PBF-LB/M. As the suggested printing parameters for this alloy, as provided in the literature, do not yield the best results, a parameter study precedes the manufacturing of the injectors. Several "critical geometries" deemed important in the injector designs were produced. Furthermore, the laser energy density was varied on a number of test specimen to achieve a low porosity and a good surface finish. Based on these results, the injector designs were

adapted.

Most importantly, an overhang angle of 60° was identified to reliably achieve a satisfactory surface quality, while lower angles would lead to irregularities for the applied printing parameters. For lower angles, deposits on top of the printed layer could form, which caused the abort of the printing process in some cases. Overhang angles $<60^\circ$ were thus avoided. This is visible in the cutaway drawings shown in figure 6. Secondly, a wall thickness of $1~\mathrm{mm}$ was deemed a lower limit for thin walls or tubes. While thinner walls could be achieved for simple structures, such as tubes, this value was chosen to produce tight and structurally sound structures with a high degree of confidence. These thin structures are mainly represented by the oxidizer lines.

All injectors are placed inside a propellant manifold, which supplies the gaseous propellant axially to the oxidizer inlet (placed up) and the fuel inlet (placed below). For the shear coaxial injector (figure 6a) and the central body shear coaxial injector (figure 6b), the propellants are fed down towards the faceplate through conical, circumferential gaps. The structure is held together by supports inside the propellant gaps. Supports are also placed near the faceplate inside the fuel and oxidizer annuli in order to increase their stiffness.

The showerhead injector (figure 6c) features a down coming oxidizer gap, analogously to the shear coaxial injectors, while the incoming fuel is led into a cavity that directs the gas flow toward the orifices inside the faceplate. The oxidizer flow is fed down through one larger tube, which splits into the individual oxidizer lines (shown in detail in figure 7). In comparison to individual oxidizer lines, starting at the inlet, this approach yields several advantages. Losses of the total pressure due to friction are reduced and less material is needed. Also, this arrangement leads to a higher mass flow through the central oxidizer orifices, as these are more directly exposed to the incoming flow. Thus, a gradient of decreasing oxidizer flow towards the combustion chamber walls can be achieved, achieving a film cooling effect.

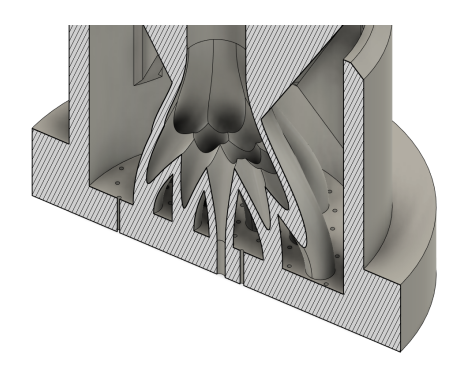


FIG 7. Showerhead injector internal fuel lines detail.

The swirl injector features a conical fuel gap, similar to the shear coaxial injectors. The oxidizer is fed to a central tube through four propellant lines that spiral downward around the central axis. The propellant lines follow a slope of 60° and feature a drop-shaped cross-section in order to comply with the overhang angle. The oxidizer flow is highlighted in figure 8. The oxidizer line geometry serves as a proof of concept of complex internal geometries inside a limited build space that could not be realized with subtracting manufac-

turing methods. The resulting, more shallow swirl angle is expected to be a compromise between a central body shear coaxial injector and a swirl injector featuring a high swirl angle. The contact area is increased and mixing is enhanced, while combustion chamber wall hotspots near the faceplate can potentially be mitigated.



FIG 8. Swirl injector internal oxidizer flow.

3.3. Manufactured injectors

Due to the previous optimization of the PBF-LB/M process with CuCr1Zr, a good manufacturing result was achieved. The injectors showed good geometrical accuracy and the problem of deposition of molten metal on top of the printed layer was avoided. However, minor irregularities in the printing of the conical overhangs led to visible scoring across all parts. These are only superficial and are not expected to have a negative impact on the structural integrity of the components. A photo of the injectors prior to post-processing, featuring a high surface roughness, is shown in figure 9.



FIG 9. Additively manufactured injectors, before postprocessing.

Using a laser scanning microscope, the arithmetic average surface roughness was measured to $87.5\,\mu\mathrm{m}.$ The surface structure is dominated by particles of similar diameter. It is assumed that smaller particles melt and larger particles do

not adhere to the surface.

As the injectors will be mounted inside a propellant manifold and radially sealed using o-rings, a low surface roughness is required. This is achieved by turning off the mantle surface. The faceplate is milled off. The burr on the coaxial injectors and the swirl injector is removed and the holes in the showerhead injector are reworked with drills of the corresponding diameter.

4. COLD-FLOW TESTING

Cold-flow testing can serve as an important step of experimental injector characterization prior to hot-fire tests. In cold-flow testing, a surrogate fluid is fed through the injector, allowing for the measurement of the pressure drop ΔP over the mass flow rate $\dot{m}.$ The pressure drop has a significant influence on flame anchoring and combustion stability in a rocket engine. A characteristic parameter that represents the pressure drop in relation to mass flow rate, fluid density and cross-sectional area is the discharge coefficient $C_d.$

(10)
$$C_d = \frac{\dot{m}}{A\sqrt{2\rho\Delta P}}$$

4.0.1. Test setup

All four injectors were tested using GN2 as a surrogate fluid. The injectors were housed within a manifold, allowing nitrogen to be directed to either the fuel or oxidizer inlet, while the opposite inlet remained closed. A ball valve was employed to adjust the cross-sectional area of the chamber's throat. Together with a pressure regulator that controlled the pressure inside the manifold, the mass flow rate and chamber pressure could be set independently. The mass flow rate was measured using a Coriolis mass flow meter. The oxygen and fuel manifold pressures were measured using Keller 23SY piezoresistive pressure transmitters. The temperature was measured at the same points using T type thermocouples. The fluid set up is shown in figure 10.

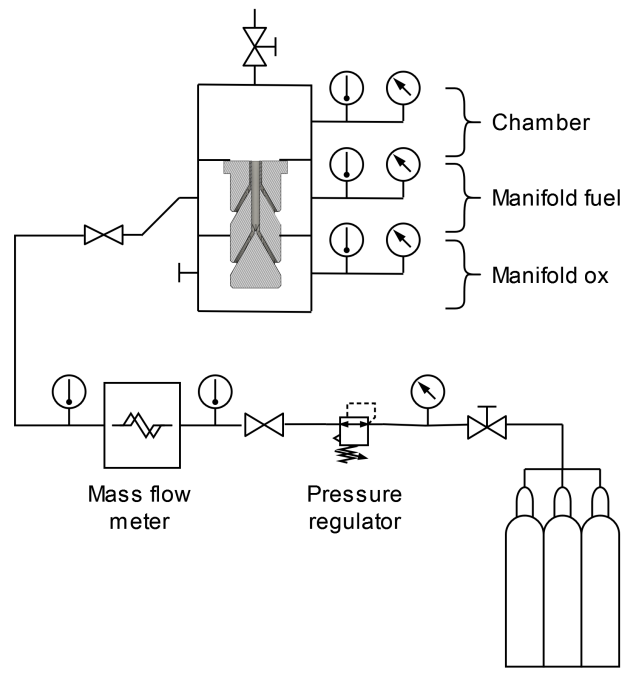


FIG 10. cold-flow setup fluid plan.

For each injector, the fuel and oxidizer lines were tested separately. Multiple measuring points with varying mass flow rate and chamber pressure were covered. A total of 80 operating points were evaluated.

Measuring points were evaluated for manifold pressures exceeding $3\,\mathrm{bar}$ during steady state intervals longer than $2\,\mathrm{s}.$ An average value within a time interval of $1\,\mathrm{s}$ was considered.

4.0.2. Results

Using the mass flow rate, cross-sectional area, and pressure drop, the discharge coefficient was calculated for all operation points using equation 10. The density was determined using a fluid property library [11] with the measured pressure and temperature.

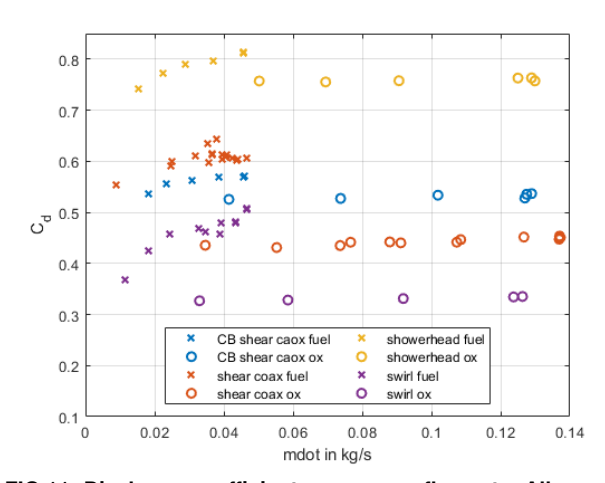


FIG 11. Discharge coefficients over mass flow rate. All operating points are shown.

The resulting discharge coefficient is plotted over the mass flow rate in figure 11 for all operation points. The values show a certain degree of scatter and a functional curve cannot be read from the data. This is also the case when considering the discharge coefficient over the manifold pressure (not shown here). From this it can be deduced that the discharge coefficient for the respective fuel and oxidizer orifices can be assumed to be constant within the considered parameters. The average values are plotted in figure 12 with their standard deviation.

The showerhead injector exhibits the highest discharge coefficient. It is 0.79 for the fuel lines and 0.76 for the oxidizer lines. This comparatively high value corresponds to a low pressure loss, which can be explained by the geometry of the injector. As can be seen in figure 7, the outlet bores have a relatively small diameter of $0.5\,\mathrm{mm}$, but also only a short length of $9\,\mathrm{mm}$. It can be assumed that the losses in the fuel dome behind it and in the inlet are comparatively low. The oxidizer lines are also distributed over small tubes towards the faceplate, with a minimum diameter of $1.4\,\mathrm{mm}$. However, the majority of the flow path leads through the downcomer with a diameter of $8\,\mathrm{mm}$, in which comparatively low pressure losses are to be expected.

Next, the shear coaxial injector and the central body shear coaxial injector are considered. The fuel line shows a value of 0.61 for the shear coaxial injector and 0.56 for the central body shear coaxial injector. This can be well explained by the design geometry: With the same cross-sectional

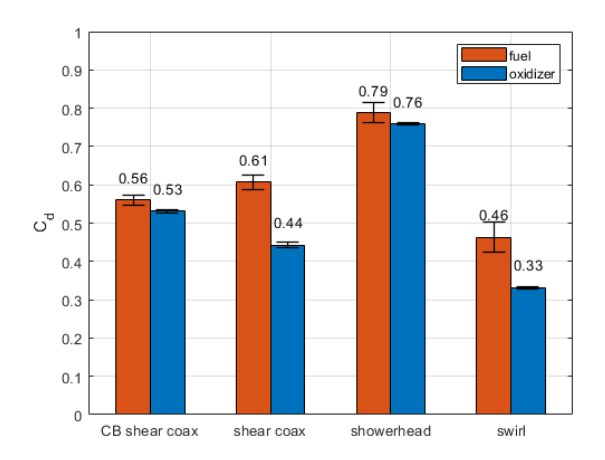


FIG 12. Discharge coefficient for the different injectors, determined experimentally in cold-flow testing. Standard deviation plotted as vertical bar.

area, the annulus of the central body shear coaxial injector is thinner, which results in a higher pressure loss. For the oxidizer lines, the shear coaxial injector exhibits a discharge coefficient of 0.44, while the central body shear coaxial has a value of 0.53. One explanation for this could be the support structures in the upper area of the shear coaxial oxidizer downcomer. These lead to a narrowing of the cross-section through which the flow passes and could potentially cause a significant pressure loss. For future analysis, the injectors will be cut open to investigate whether further production-related constrictions can be identified. An investigation of the internal fuel lines may shed light on the comparatively low discharge coefficients of the shear coaxial injectors.

The swirl injector exhibits the lowest discharge coefficients with 0.49 for the fuel lines and 0.33 for the oxidizer lines. As the oxidizer lines are constructed as long and narrow spiralling tubes, the high pressure drop appears understandable. The fuel line geometry is similar to the shear coaxial injectors, forming a cone-shaped circumferential gap. The low discharge coefficient in comparison to the shear coaxial injectors cannot be easily explained. While the annulus diameter is higher, the same is true for the cross-sectional area. Investigations of the cut component might shed light on constrictions due to manufacturing.

For all injectors, the fuel discharge coefficient is higher than the oxidizer discharge coefficient. It should be noted that, for the chosen mixture ratio and cross-sectional areas, the opposite case would be beneficial in order to achieve similar injector inlet pressures for fuel and oxidizer. For future design iterations, a higher ratio of the oxidizer to fuel cross-sectional areas will be chosen for this reason.

5. CONCLUSION

The goal of this preliminary study was the dimensioning, design, and manufacturing of injectors for a small $500\,\mathrm{N}$ thruster utilizing GO2/GCH4. The injectors were to be manufactured by PBF-LB/M, utilizing CuCr1Zr. For dimensioning the injectors, a momentum flux ratio and oxidizer and fuel injection velocities were defined with reference to existing studies on small GO2/CH4 thrusters. Thus, the

required injection surface cross-sectional areas could be determined. To determine an estimated mixture efficiency and to relate the performance in the space of possible face-plate geometries, a simplified cold-flow mixing model was used. Four injectors were manufactured: a shear coaxial injector, a central body shear coaxial injector, a showerhead injector and a swirl injector. The components showed good geometrical accuracy. The external surfaces were post-processed due to the relatively high surface roughness.

Cold-flow testing of all injectors was performed using GN2 to determine the respective discharge coefficients. These values will provide valuable insights for the next iteration of injectors which will be subjected to hot-fire testing. The internal propellant lines will be inspected to evaluate the surface roughness and the overall quality achieved in the AM process by cutting open the specimens, shedding light on the pressure losses inside the propellant lines.

In this preliminary study, the feasibility of producing injectors for a small GO2/GCH4 rocket thruster using PBF-LB/M with CuCr1Zr could be demonstrated. Findings of this study will guide the design of the next iteration of additively manufactured injectors, which will be subjected to cold-flow and hot-fire testing. Intricate internal structures can be produced with high copper alloys, allowing rocket engine injectors that combine good thermal, structural, and flow dynamic properties

6. ACKNOWLEDGEMENTS

I would like to thank the DeltaOrbit team members Dr. Christian Bauer, Felix Schily, and Dr. Rahand Dalshad for their invaluable guidance and assistance.

Contact address:

justus.caspar@tu-braunschweig.de

References

- [1] michele.di.magno@esa.int. Building the european space logistics ecosystem for in-space transportation. https://commercialisation.esa.int/2022/09/building-the-european-space-logistics-ecosystem-for-in-space-transportation-2/.
- [2] Sebastian Soller, Volker Kaufmann, and Frederic Laithier. Design and testing of liquid propellant injectors for additive manufacturing. Artwork Size: 10 pages Medium: PDF Publisher: Proceedings of the 7th European Conference for Aeronautics and Space Sciences. Milano, Italy, 3-6 july 2017. DOI: 10.13009/EUCASS2017-306.
- [3] Dmitry I Suslov, Jan Haubrich, Jan Haemisch, Katia J Artzt, Juri Munk, Wolfgang Armbruster, Justin S Hardi, and Jan C Deeken. Development and qualification of a laser powder bed fusion manufactured 25 kN LOX/LNG regeneratively cooled thrust chamber produced from CuCr1zr-alloy.
- [4] Jan Reuter, Rahand Dalshad, and Christian Bauer. Development and test of a methalox engine injector with distributed micro-injection.
- [5] T. Fiedler, M. Jähnig Domingues, C. Winter, and J. Rösler. High conductive copper alloys for ad-

- ditive manufacturing. ISSN: 2363-9512, 2363-9520. DOI: 10.1007/s40964-023-00527-3.
- [6] D. F. Calhoon, J. I. Ito, and D. L. Kors. Investigation of gaseous propellant combustion and associated injector/chamber design guidelines.
- [7] Sanford Gordon and Bonnie J. McBride. Computer program for calculation of complex chemical equilibrium compositions and applications. part 1: Analysis.
- [8] Jack H. Rupe. The liquid-phase mixing of a pair of impinging streams.
- [9] Fernanda Winter, Simona Silvestri, Maria Palma Celano, and Oskar Haidn. High-speed and emission imaging of a coaxial single element GOX/GCH4 rocket combustion chamber. page 10 pages. Artwork Size: 10 pages Medium: PDF Publisher: Proceedings of the 7th European Conference for Aeronautics and Space Sciences. Milano, Italy, 3-6 july 2017. DOI: 10.13009/EUCASS2017-340.
- [10] Nikolaos Perakis, Daniel Rahn, Daniel Eiringhaus, and Oskar J. Haidn. Heat transfer and combustion simulation of a 7-element GOX/GCH4 rocket combustor. In 2018 Joint Propulsion Conference. American Institute of Aeronautics and Astronautics. ISBN: 978-1-62410-570-8. DOI: 10.2514/6.2018-4554.
- [11] Ian H. Bell, Jorrit Wronski, Sylvain Quoilin, and Vincent Lemort. Pure and pseudo-pure fluid thermophysical property evaluation and the open-source thermophysical property library CoolProp. 53(6):2498–2508. _eprint: http://pubs.acs.org/doi/pdf/10.1021/ie4033999.